

4-(Phenoxy) and 4-(benzyloxy)benzamides as potent and selective inhibitors of mono-ADP-ribosyltransferase PARP10/ARTD10

Sudarshan Murthy¹, Jenny Desantis², Patricia Verheugd³, Mirko M. Maksimainen¹, Harikanth Venkannagari¹, Serena Massari², Yashwanth Ashok¹, Ezeogo Obaji¹, Yves Nkizinkinko¹, Bernhard Lüscher³, Oriana Tabarrini² & Lari Lehtiö^{1,*}

¹Biocenter Oulu and Faculty of Biochemistry and Molecular Medicine, University of Oulu, Oulu, Finland

²Department of Pharmaceutical Sciences, University of Perugia, 06123 Perugia, Italy

³Institute of Biochemistry and Molecular Biology, RWTH Aachen University, 52074 Aachen, Germany

*Address correspondence to L.L.: phone: +358 2 9448 1169; E-mail: lari.lehtio@oulu.fi

ABSTRACT

Human Diphtheria toxin-like ADP-ribosyltransferases (ARTD) 10 is an enzyme carrying out mono-ADP-ribosylation of a range of cellular proteins and affecting their activities. It shuttles between cytoplasm and nucleus and influences signaling events in both compartments, such as nuclear factor kappa-light-chain-enhancer of activated B cells (NF- κ B) signaling and S phase DNA repair. Furthermore, overexpression of ARTD10 induces cell death. We recently reported on the discovery of a hit compound, OUL35 (compound **1**), with 330 nM potency and remarkable selectivity towards ARTD10 over other enzymes in the human protein family. Here we aimed at establishing a structure-activity relationship of the OUL35 scaffold, by evaluating an array of 4-phenoxybenzamide derivatives. By exploring modifications on the linker between the aromatic rings, we identified also a 4-(benzyloxy)benzamide derivative, compound **32**, which is potent ($IC_{50} = 230$ nM) and selective, and like OUL35 was able to rescue HeLa cells from ARTD10-induced cell death. Evaluation of an enlarged series of derivatives produced detailed knowledge on the structural requirements for ARTD10 inhibition and allowed the discovery of further tool compounds with submicromolar cellular potency that will help in understanding the roles of ARTD10 in biological systems.

Key Words:

ADP-ribosylation; PARP; ARTD; Inhibitor; Structure-Activity Relationship

1. Introduction

ADP-ribosylation is a post translational reversible protein modification catalysed in human cells by dedicated ADP-ribosyltransferase enzymes and some sirtuins [1]. ADP-ribosyltransferases share homology to bacterial toxins and they can be divided into membrane anchored cholera toxin-like (ARTCs) and mainly soluble diphtheria toxin-like (ARTDs or PARPs) enzymes. The ARTD family includes 17 protein modifying enzymes that share a conserved catalytic domain responsible for ADP-ribosylation activity [2–4]. Based on the catalytic activity, the members of the human ARTDs family are further categorised into transferases that are capable of synthesizing polymers of ADP-ribose (pARTDs) and mono-ADP-ribosyltransferases (mARTDs). The key difference between the enzymes is in the ‘H-Y-E’ (His-Tyr-Glu) motif where Glu is replaced by a hydrophobic residue in mARTDs. The lack of the Glu residue limits the activity of mARTD to mono-ADP-ribosylation (MARylation) of a target residue without poly-APD-ribose formation [5]. mARTDs are involved in various cellular activities, including transcriptional regulation, immunity and inflammation, stress response, and DNA damage response [6]. Some of these functions have been linked to diseases such as cancer and thus the relevant enzymes represent potential therapeutic targets [7,8].

ARTD10 belongs to the mARTD class and it was the first enzyme experimentally demonstrated to be a true mARTD [5]. ARTD10 was first described as a novel c-Myc interacting partner and it was shown that it ADP-ribosylates itself and also core histones [9]. The catalytic motif of ARTD10 contains an Ile, but when it was mutated to Glu, analogous to pARTDs, it did not transform ARTD10 to a polymerase indicating that there are further differences in addition to the simple amino acid substitution [5,10]. In addition to the C-terminal catalytic domain, ARTD10 contains several other domains and motifs, including an RNA recognition motif (RRM), two ubiquitin interacting motifs (UIMs) as well as nuclear localization and export sequences (NLS and NES) [5,9]. Within the catalytic domain there is a small sequence motif, a PIP box, enabling interaction with proliferating cell nuclear antigen (PCNA) [11]. The domains and motifs allow ARTD10 to interact with various

proteins and enable it to function in apoptosis, signalling, DNA repair, and transcription. ARTD10 shuttles between both cytoplasm and nucleus and it is hypothesized that the RRM may be involved in control of RNA processing in programmed cell death [12,13].

Protein microarray studies have shown that many of the ARTD10 target proteins are kinases, receptors and growth factors [14]. ARTD10 has been shown to interact with K63-linked poly-ubiquitin chains (K63-pUb) through its two UIMs. K63-pUb serves as a scaffold in several signalling pathways, including in signal transduction by NF- κ B. ARTD10 interaction with K63-pUb facilitates ADP-ribosylation of nuclear factor NF- κ B essential modulator (NEMO) and prevents its poly-ubiquitination. In turn this results in reduced activation of inhibitor of κ B kinases, which prevents NF- κ B-dependent gene transcription [15]. ARTD10 is also involved in modulating glycogen synthase kinase (GSK3 β) activity, which has functions in Wnt signalling, metabolism, neural development, and tumorigenesis [14]. During S phase DNA repair, ARTD10 is recruited by PCNA to DNA damage sites where MARYlation activity is required to promote translesion DNA synthesis in the event of replication fork stalling [11]. Recently, it has been reported that a deficiency in ARTD10 correlates with severe developmental delays in a patient and that the extracted patient cells are sensitive to replication stress induced by hydroxyurea and display enhanced DNA damage-induced apoptosis [16]. It implies that the DNA repair failure could be due to the loss of ADP-ribosylation of DNA repair proteins [16].

We described earlier a robust screening method for ARTD10 inhibitors and used it to discover a hit compound, OUL35 (further referred to as compound **1**, **Figure 1A**), which turned out to be a potent ($IC_{50} = 330$ nM) and selective ARTD10 inhibitor [17,18]. Compound **1** is also able to enter cultured cells and inhibit ARTD10-dependent cellular processes. Docking-based structural analysis indicated that compound **1** extends toward the so called “acceptor site” where a potential substrate protein would bind to be ADP-ribosylated (**Figure 1B,C**). Compound **1** has two symmetrical aromatic benzamide moieties designated hereafter as anA-ring binding to the nicotinamide binding site and a

B-ring extending towards the acceptor site. With the aim to evaluate the structural requirements for activity and selectivity of compound **1**, we analyzed a set of its analogs for ARTD10 inhibition. We used commercially available compounds and synthesized the missing key compounds in order to obtain a complete picture of the structure–activity relationship (SAR). We demonstrate that only a small electron donating ether substituent at the *p*-position of the A-ring benzamide is needed for ARTD10 micromolar inhibition, but larger substituents enhanced the potency while maintaining ARTD10 selectivity. Also the cellular efficacy was improved with the best compounds that showed submicromolar potency in a colony formation assay.

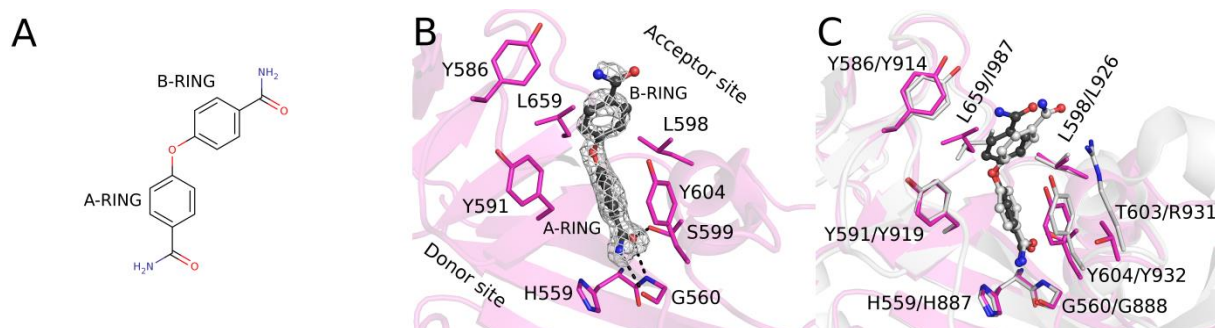
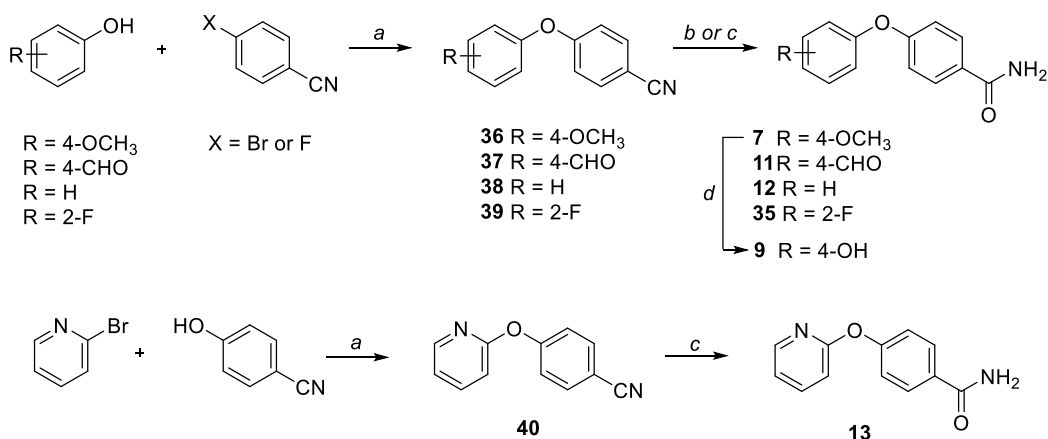


Figure 1. Binding of compound **1** to the active site. **A)** Chemical structure of **1** with the aromatic rings indicated as A- and B-rings. **B)** Crystal structure **1** bound to the nicotinamide pocket of ARTD7 (Y598L). Sigma A weighted omit F_o-F_c electron density map is coloured in white and contoured at 3.0σ . Amino acid residues and **1** are coloured in magenta and black, respectively. A- and B-rings of **1** are indicated. Hydrogen bonds between **1** and residues are indicated by black dash lines. **C)** Superimposition of the nicotinamide pockets of the ARTD7 (Y598L) complex structure (colored in magenta) with the modelled binding pose in ARTD10 (colored in light grey). Residues for ARTD7/ARTD10 are labelled.

2. Chemistry

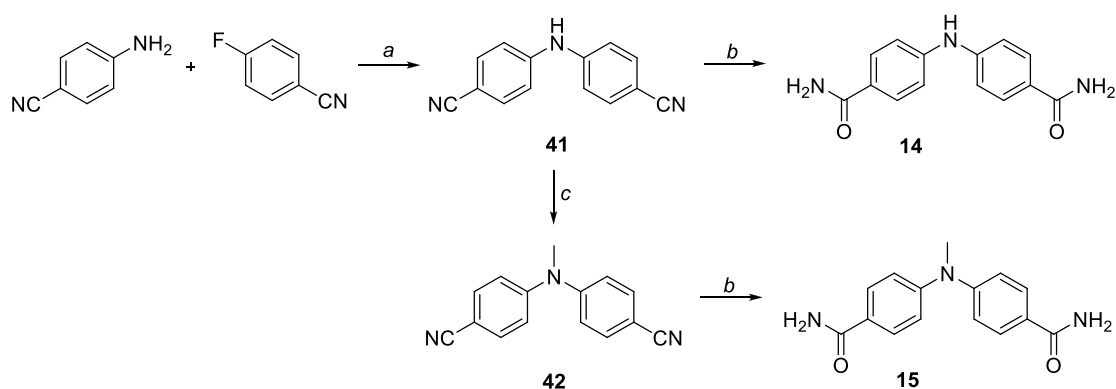
Among the studied compounds, the synthesis of derivatives **7**, **9**, **11-17**, **19**, and **35** was carried out according to the reactions depicted in Schemes 1-4. 4-Phenoxybenzamides **7**, **9**, **11**, **12**, and **35**

(Scheme 1) were obtained through a first coupling reaction between the appropriate phenols and 4-fluorobenzonitrile furnishing intermediates **36** [19] **37** [20], **38** [19], and **39** [21], which were then converted into their corresponding benzamides **7** [22], **11** [23], **12** [24], and **35**, respectively, by using H₂O₂ and K₂CO₃ in DMSO or H₂SO₄. *O*-Demethylation of the methoxy derivative **7**, performed with BBr₃ in dry CH₂Cl₂, led to the corresponding hydroxyl derivative **9**. An analogous procedure was applied for the preparation of compound **13** (Scheme 1), by reacting 4-hydroxybenzonitrile and 2-bromopyridine yielding the benzonitrile intermediate **40** [25], which was then hydrated under acid-catalyzed conditions affording benzamide derivative **13**.



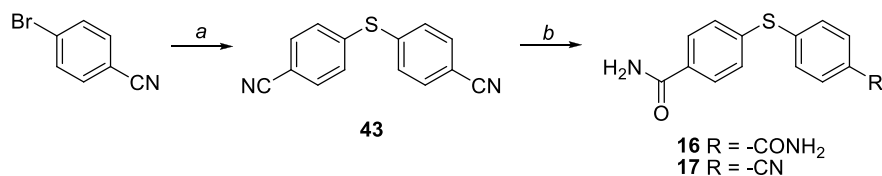
Scheme 1. Synthesis of compounds **7**, **9**, **11**, **12**, and **35**. *Reagents and conditions:* (a) KOtBu, dry DMSO, 160° C; (b) H₂O₂ 30%, K₂CO₃, DMSO, rt; (c) H₂SO₄ conc, 60° C; (d) BBr₃, dry CH₂Cl₂, rt.

Analogously, derivatives **14** and **15**, in which a nitrogen atom replaced the oxygen linker, were synthesized starting with the preparation of intermediate **41** [26] obtained by reacting 4-aminobenzonitrile and 4-fluorobenzonitrile (Scheme 2). Methylation of intermediate **41** to compound **42** [27] was performed with MeI and K₂CO₃. The successive H₂O₂ mediated conversion of the nitrile groups of compounds **41** and **42** yielded the corresponding amide derivatives **14** and **15**, respectively.



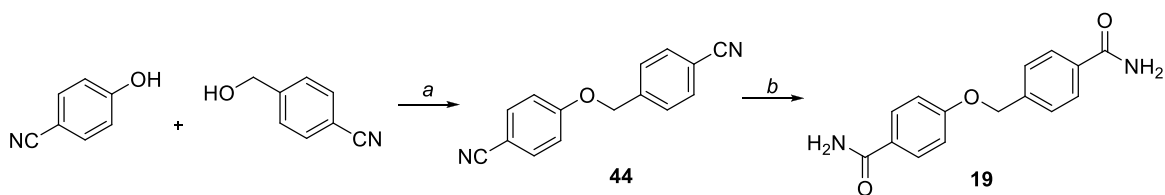
Scheme 2. Synthesis of compounds **14** and **15**. *Reagents and conditions:* (a) KOtBu, dry DMSO, 160° C; (b) H₂O₂ 30%, K₂CO₃, DMSO, rt; (c) MeI, K₂CO₃, dry DMF, rt.

Derivatives **16** and **17**, in which the oxygen linker was replaced by a sulfur atom, were prepared by treating 4-bromobenzonitrile in the presence of sulfur, CuI and Cs₂CO₃ in dry DMF, furnishing derivative **43** [28], which in turn was converted into target compounds by reaction with different equivalents of H₂O₂ (Scheme 3).



Scheme 3. Synthesis of compounds **16** and **17**. *Reagents and conditions:* (a) S₈, CuI, Cs₂CO₃, dry DMF, 100° C; (b) H₂O₂ 30%, K₂CO₃, DMSO, rt.

Finally, 4-(benzyloxy)benzamide derivative **19** was prepared by applying a Mitsunobu reaction between 4-hydroxybenzonitrile and 4-(hydroxymethyl)benzonitrile, followed by H₂O₂ mediated conversion of the resulting dibenzonitrile intermediate **44** [29] (Scheme 4).



Scheme 4. Synthesis of compound **19**. *Reagents and conditions:* (a) Ph_3P , DIAD, dry THF; (b) H_2O_2 30%, K_2CO_3 , DMSO, rt.

3. Results

3.1. Structural analysis of the binding site

We previously reported on the discovery of compound **1** (OUL35) as a first-in-class inhibitor of ARTD10 (**Figure 1A**) [15]. Based on molecular docking and mutagenesis studies, we proposed that the compound would bind to the nicotinamide binding pocket of ARTD10 analogously to previously characterized ARTD/PARP inhibitors, but it would extend to the so called “acceptor site”. The acceptor site was identified by Ruf and co-workers as the location where the target protein to be ADP-ribosylated is expected to interact [30]. In order to gain further confidence on its binding mode, we determined a crystal structure of compound **1** in complex with ARTD7 (Y598L) at 1.6 Å resolution (**Figure 1B**). This ARTD7 protein is a gain-of-binding mutant containing the mutation Y598L that corresponds to the Leu926 in ARTD10. The mutation allows the binding of **1** with similar affinity as ARTD10 itself ($\text{IC}_{50} = 300 \text{ nM}$), while we have not been able to get a co-crystals of ARTD10 with **1** [17]. The crystal structure contains two protein molecules in the asymmetric unit and compound **1** had well defined electron density in one of the active sites (**Figure 1B**). However, in the second molecule compound **1** is only partially visible based on the electron density (**Figure S1**). The superimposition of protein chains suggests that the binding of compound **1** induces a disorder in the D-loop. In molecule binding **1**, the residues between Cys578 and Asn582 lack electron density and therefore they are not included in the model. In the second protein molecule, the D loop is completely visible but its conformation does not allow compound **1** to bind because the loop would clash with

the compound (**Figure S1A**). Furthermore, inspection of the crystal packing reveals that a neighboring protein molecule limits the mobility of the D-loop in molecule not binding **1** (**Figure S1B**).

The structure revealed that compound **1** is, as predicted, bound to the nicotinamide pocket between the two tyrosine residues Tyr591 and Tyr604. The A-ring benzamide forms three hydrogen bonds with Gly560 and Ser599, as typically observed for ARTD inhibitors (**Figure 1B**). Compound **1** extends from the binding pocket towards the acceptor site and the B-ring benzamide is located between Leu598 and Leu659. Leu659 is the hydrophobic residue of the H-Y-E motif, which in pARTD is a Glu that would clash with the compound and explains why **1** does not inhibit pARTDs. This crystal structure superimposes well with the predicted binding mode of compound **1** to the active site of ARTD10 (**Figure 1C**). In addition to the gain-of-binding mutation (Y598L), ARTD7 contains a Thr603, while the corresponding residue in ARTD10 is Arg in position 931. This residue could modulate the compound potency and, indeed, was later identified to form a key interaction when analogs of **1** were tested for ARTD10 inhibition.

3.2. Selection and design of compound 1 analogs

A first important SAR insight was the finding that when amide moieties of compound **1** were mono- and di-methylated, the compounds completely lost the ARTD10 inhibitory activity [17]. This is in agreement with the crystal structure revealing that methylation of the A-ring would destroy hydrogen bonding at the nicotinamide binding site (**Figure 1B**). In order to understand the structural requirements for the anti-ARTD10 activity of compound **1**, we assayed a panel of commercially available analogs and complemented the series with designed and synthesized derivatives. A moiety like benzamide mimicking nicotinamide is found in most of the ARTDs inhibitors and it is a key feature anchoring the compounds to the active site. We therefore decided to keep one of the benzamides of compound **1** (A-ring) and modified other parts of the molecule to study minimal

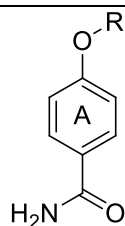
structural requirements for ARTD10 inhibition (compounds **2-6**, **Table 1**), the role of the substituent on the B-ring, as well as the role of the linker between the two aromatic rings (**7-35**, **Tables 2-4**).

3.3. Minimum requirements for an ARTD10 inhibitor

To study the importance of the benzamide rings in hit compound **1**, the B-ring was deleted in compound **2** and replaced by various alkyl substituents in compounds **3-6** (**Table 1**). The small 4-hydroxybenzamide **2** did not inhibit ARTD10 significantly at 10 μ M concentration. This is analogous to what was previously reported for the structurally related ARTD inhibitor 3-aminobenzamide [18]. In contrast, the *O*-methyl group in **3** was enough to achieve an IC_{50} of 2.8 μ M for ARTD10 inhibition. Increasing the length of the alkyl group by one atom, as in compound **4**, slightly decreased potency, while isopropyl and cyclobutyl derivatives gave 1.3 μ M and 720 nM inhibitors **5** and **6**, respectively. Together, the data indicated that even a small *O*-linked alkyl group would be enough to gain ARTD10 inhibitory activity, while a bulkier substituent would lead to lower IC_{50} values and thus higher inhibitory potency. Indeed, the region in the catalytic domain leading to the acceptor site is hydrophobic due to the surrounding amino acid residues Tyr, Leu and Ile residues (**Figure 1C**) explaining why an alkyl substituent is suitable at this position.

Table 1. Exploration of the minimal compound inhibiting ARTD10. Inhibition % at 10 μ M

concentration or the measured IC₅₀ (pIC₅₀ ± SEM, n=3) is reported.



Cmpd	R	IC ₅₀ (pIC ₅₀ ± SEM) / inh. %
1	- <i>p</i> -CONH ₂ Ph	330 nM
2	-H	27%
3	-CH ₃	2.8 μM (5.56 ± 0.19)
4	-CH ₂ CH ₃	3.5 μM (5.47 ± 0.04)
5	-CH(CH ₃) ₂	1.3 μM (5.90 ± 0.05)
6	- <i>c</i> -butyl	720 nM (6.14 ± 0.06)

3.4. Role of the *p*-substituent of the B-ring

As we did not observe an increase in potency compared to **1**, we maintained the B-ring focusing on the nature of the *p*-substituent. Replacement of the amide moiety of compound **1** by methoxy (**7**) resulted in an IC₅₀ of 1.4 μM and similar micromolar affinities were observed for amine (**8**) and hydroxyl (**9**) derivatives (**Table 2**). On the other hand, the carboxylic acid derivative (**10**) had an improved IC₅₀ of 180 nM, but the presence of an aldehyde moiety (**11**) increased the IC₅₀ to 710 nM. These data indicated that while the amide is not strictly required for inhibition, a carbonyl feature seems important for potency. Moreover, a hydrogen bond donor in the B-ring is not required as shown by the carboxyl acid derivative **10** that results in even better potency potentially due to ionic interaction with Arg931. In the docking model of ARTD10 with compound **1** (**Figure 1C**), we observed a putative hydrogen bond of Arg931 with the carbonyl. Mutating Arg931 to Ala resulted in a drop in potency (IC₅₀ 600 nM) similarly to the compounds lacking this interaction [17]. If the *p*-

substituent is removed (**12**), the potency equals that of the small alkyl substituted compounds (**Table 1**) indicating that the aromatic character is not required at the B-ring. Replacement of the whole benzamide B-ring with a 2-pyridine (**13**) was very detrimental to the inhibition perhaps due to unfavourable interaction with Leu929 (**Figure 1C**). Together the results indicate that a phenyl B-ring is not mandatory, but when suitably substituted with a carbonyl group at the *p*-position, such as carboxylic acid, amide, and to some extent aldehyde, it provides a potent ARTD10 inhibitor. Docking of **10** and **11** to the active site of ARTD10 suggests similar binding modes to that of compound **1**: A-ring benzamide binds to the nicotinamide pocket, while the B-ring extends towards the acceptor site (**Figure S2A,B**).

Table 2. Exploration of the 4-substituent in the B-ring. Inhibition % at 10 μM concentration or the measured IC_{50} ($\text{pIC}_{50} \pm \text{SEM}$, $n=3$) is reported.

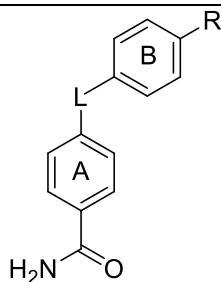
Cmpd	R	X	IC_{50} ($\text{pIC}_{50} \pm \text{SEM}$)
1	-CONH ₂	CH	330 nM
7	-OCH ₃	CH	1.4 μM (5.86 ± 0.19)
8	-NH ₂	CH	1.3 μM (5.90 ± 0.11)
9	-OH	CH	1.8 μM (5.76 ± 0.13)
10	-COOH	CH	180 nM (6.73 ± 0.05)
11	-CHO	CH	710 nM (6.21 ± 0.21)
12	-H	CH	1.1 μM (5.94 ± 0.07)
13	-H	N	49%

3.5. Linker modifications

The oxygen linker in **1** restricts the geometry of the symmetric *O*-linked benzamide rings and the angle between them to approximately 111°. In order to evaluate the requirement for the particular geometry of this feature, we studied alternative linking moieties (**Table 3**). Initially, the oxygen atom was replaced by other heteroatoms such as nitrogen (**14** and **15**), sulfur (**16** and **17**), and phosphorus (**18**). All the substitutions were detrimental indicating that the geometry between the nicotinamide mimicking benzamides was critical for ARTD10 inhibition.

Lower potency ($IC_{50} = 2 \mu M$) was observed also when longer and more flexible $-OCH_2-$ was used as linker (compound **19**), while the same linker coupled with the unsubstituted phenyl ring led to slightly improved potency for compound **20** ($IC_{50} = 1.4 \mu M$). The longer linker would push the B-ring more towards the acceptor site possibly explaining this observation (**Figure 1**). Based on this data, two additional unsubstituted analogs (**21** and **22**), characterized by an ester or an ethylene glycol linker, respectively, were also tested, but they were less active than **20**. Additional compounds modified at both the linker and at the C-4 substituent (**23**, **24** and **25**) were almost completely inactive. Altogether these data indicated that changing the linking moiety decreased the potency to varying degrees. Thus an ether is required for potent activity revealing the linker geometry as a critical factor for the inhibitor potency. These data also highlighted that while the presence of a suitable substituent at the *p*-position of the 4-phenoxybenzamide B-ring grants potent ARTD10 inhibitory activity, the 4-(benzyloxy)benzamides, characterized by the longer $-OCH_2-$ linker, are less tolerant to a *p*-substituent.

Table 3. Exploration of the linker between the aromatic rings. Inhibition % at 10 μM concentration or the measured IC_{50} ($\text{pIC}_{50} \pm \text{SEM}$, $n=3$) is reported.

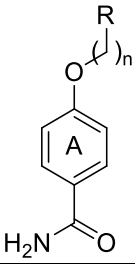
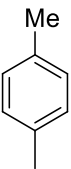
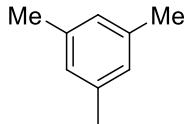
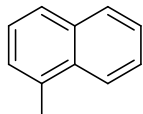
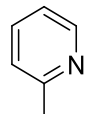
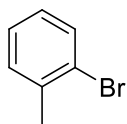
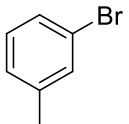
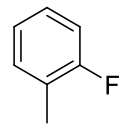
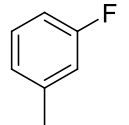
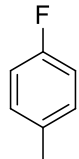
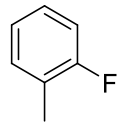


Cmpd	L	R	IC_{50} ($\text{pIC}_{50} \pm \text{SEM}$) / inh. %
14	-NH-	-CONH ₂	0%
15	-N(CH ₃)-	-CONH ₂	26%
16	-S-	-CONH ₂	30%
17	-S-	-CN	16%
18	-PO(CH ₃)-	-CONH ₂	0%
19	-OCH ₂ -	-CONH ₂	2.0 μM (5.64 ± 0.11)
20	-OCH ₂ -	-H	1.4 μM (5.87 ± 0.18)
21	-OCO-	-H	7.3 μM (5.14 ± 0.02)
22	-OCH ₂ CH ₂ O-	-H	1.9 μM (5.71 ± 0.13)
23	-CO-	-NO ₂	24%
24	-OCH(CH ₃)-	-CH(CH ₃) ₂	16%
25	-CH ₂ O-	-OCH ₂ CH ₃	0%

Thus, we decided to test if the potency of the 4-(benzyloxy)benzamides could be enhanced by placing different substituents in the various positions of the B-ring. The presence of a *p*-methyl substituent (**26**) lowered the potency to 9.3 μM , which however slightly increased to 4.5 μM when two methyl groups were placed at *m*-positions (**27**) (**Table 4**). The acceptor site is located on the surface of the protein and it contains hydrophilic side chains explaining why lipophilic methyl groups would not be

preferred on the B-ring. In contrast however, a bulky naphthyl group in **28** was tolerated resulting in an IC_{50} of 1.4 μ M similar to **20**. While the 2-pyridyl ring decreased drastically potency in the 4-phenoxybenzamide derivative **12** (Table 2) for the longer 4-(benzyloxy)benzamide scaffold it resulted in a same IC_{50} as a phenyl B-ring (**29**, Table 4). Halogen substituents on the B-ring resulted in varying changes in IC_{50} values. *o*- (**30**) and *m*-Bromo (**31**) derivatives were weak ARTD10 inhibitors with IC_{50} values of 3.8 μ M and 2.2 μ M, respectively. Differently, an *o*-fluoro substituted derivative (**32**) was the most potent compound identified in this study with IC_{50} of 230 nM, which is in strong contrast to IC_{50} values of *m*- (**33**, IC_{50} = 3.3 μ M) and even more of *p*-fluoro (**34**, IC_{50} = 7.9 μ M) derivatives. The data collected analyzing all the 4-(benzyloxy)benzamides showed that the nature of the B-ring strongly modulates the activity, the *p*-position was confirmed as the less suitable to accommodate substituents, and a proper group can confer potent activity as in the case of *o*-fluoro derivative **32**. The interesting activity of **32** prompted the synthesis of the 4-(phenoxy)benzamide analog **35**, which however was less active (IC_{50} = 1.7 μ M) confirming the different SAR for 4-(benzyloxy) and 4-(phenoxy)benzamides. The *o*-fluoro substituent of **35** actually lowered the potency of the corresponding 4-phenoxy(benzamide) **12** (1.7 μ M and 1.1 μ M, respectively).

Table 4. Substituents in the B-ring. Inhibition % at 10 μM concentration or the measured IC_{50} ($\text{pIC}_{50} \pm \text{SEM}$, $n=3$) is reported.

							
Cmpd	R	n	IC_{50} ($\text{pIC}_{50} \pm \text{SEM}$)	Cmpd	R	n	IC_{50} ($\text{pIC}_{50} \pm \text{SEM}$)
26		1	9.3 μM (5.03 \pm 0.12)	27		1	4.5 μM (5.34 \pm 0.03)
28		1	1.4 μM (5.84 \pm 0.04)	29		1	1.35 μM (5.87 \pm 0.16)
30		1	3.8 μM (5.42 \pm 0.13)	31		1	2.2 μM (5.66 \pm 0.09)
32		1	230 nM (6.63 \pm 0.25)	33		1	3.3 μM (5.48 \pm 0.13)
34		1	7.9 μM (5.10 \pm 0.08)	35		0	1.7 μM (5.77 \pm 0.16)

Based on docking, the B-ring in 4-(benzyloxy)benzamide extends to the acceptor site but is in a different orientation compared to the more conformationally restricted 4-(phenoxy)benzamides (**Figure S2C**). The fluorine atom in **32** could enhance the compound interaction with the aromatic side chain of Tyr919 with CH-F distance of 2.8 Å in the docking model.

3.6. Profiling for inhibitor selectivity

The initial hit compound **1** had shown good selectivity for ARTD10 compared to the other tested ARTD/PARP enzymes [17] and we wanted to test whether the new compounds **10**, **11**, and **32** retained this property (**Table 5**). We also included compound **3** in the profiling to assess minimal requirements for ARTD10 selectivity. Overall, the best ARTD10 inhibitors are also selective towards it and they are all poor inhibitors of pARTDs ARTD1, 2, 5 and 6. Compound **10** inhibits also ARTD7/PARP15 ($IC_{50} = 2.6 \mu M$), while **11** was remarkably selective towards ARTD10. It could be expected that the longer and more flexible -OCH₂- linker in **32** would cause poor selectivity, but we only observed some inhibition of ARTD7/PARP15 and ARTD8/PARP14. We did not observe much stabilization of ARTD9 and ARTD13 in differential scanning fluorimetry and only compound **10** had over 1 degree T_m shift for ARTD9, while there was a clear correlation with the T_m shift and IC₅₀ values for ARTD10 (**Table 5**, **Figure S3A,B**). Surprisingly, the minimalistic compound **3** was also selective towards ARTD10 suggesting that the oxygen in the linker is a key element for inhibitor selectivity and it can be further modulated by an aromatic B-ring and its substituents.

Table 5. IC50 and thermal stabilization by hit compounds against other ARTD family members. Thermal stabilization was measured at 100 μ M.

	1[#]	3	10	11	32
ARTD1/PARP1	>100 μ M	57 μ M	>100 μ M	>100 μ M	>100 μ M
ARTD2/PARP2	>100 μ M	77 μ M	>100 μ M	>100 μ M	>100 μ M
ARTD3/PARP3	>100 μ M	>100 μ M	>100 μ M	86 μ M	>100 μ M
ARTD4/PARP4	23 μ M	65 μ M	>100 μ M	>100 μ M	>100 μ M
ARTD5/TNKS1	>100 μ M	>100 μ M	>100 μ M	>100 μ M	>100 μ M
ARTD6/TNKS2	>100 μ M	>100 μ M	>100 μ M	>100 μ M	>100 μ M
ARTD7/PARP15	>10 μ M	>10 μ M	2.6 μ M	> 10 μ M	3.3 μ M
ARTD8/PARP14	23 μ M	>10 μ M	> 10 μ M	> 10 μ M	~ 10 μ M
ARTD9/PARP9*	0.72 \pm 0.13	0.15 \pm 0.38	1.2 \pm 0.60	0.04 \pm 0.44	0.76 \pm 0.28
ARTD10/PARP10	330 nM	2.8 μ M	180 nM	710 nM	230 nM
ARTD10/PARP10*	3.8 \pm 0.10	2.76 \pm 1.0	5.21 \pm 0.89	3.60 \pm 0.80	4.20 \pm 0.60
ARTD12/PARP12	> 10 μ M	>10 μ M	> 10 μ M	>10 μ M	> 10 μ M
ARTD13/PARP13*	0.40 \pm 0.08	0.44 \pm 0.16	0.72 \pm 0.13	0.49 \pm 0.18	0.37 \pm 0.12
ARTD15/PARP16	4.2 μ M	> 10 μ M	>10 μ M	> 10 μ M	> 10 μ M

* ΔT_m (DSF), $^{\circ}$ C \pm SD; [#]values taken from Venkannagari et al [17].

3.7. Cell activities of the most potent compounds

From the whole set of compounds, 4-(phenoxy)benzamides **10** and **11** and 4-(benzyloxy)benzamide **32** showed highest/best ARTD10 inhibition, and therefore they were selected for further studies. We tested whether they could rescue HeLa cells from ARTD10 induced cell death (**Figure 2A**), as previously shown by compound **1** [17]. This assay demonstrates whether the compounds are able to enter cells and inhibit overexpressed ARTD10 enzyme, which depends on enzymatic activity promotes/causes cell death. The carboxylic acid derivative **10** was completely inactive in the colony

formation assay (**Figure 2B**), while the aldehyde derivative **11** ($IC_{50} = 1 \mu M$) had similar cellular activity as **1** ($IC_{50} = 1.35 \mu M$) [15] (**Figure 2C, D**). The *o*-fluoro 4-(benzyloxy)benzamide derivative **32** ($IC_{50} = 2 \mu M$) was slightly less active than compound **1** (**Figure 2C,D**). At the highest concentration of **11** and **32** the ARTD10 effect was fully reverted and no toxic effect in control cells expressing the catalytically inactive ARTD10-G888W was observed (**Figure 2C**). Most probably, the lack of activity of compound **10** is due to its inability to enter cells and engage with ARTD10 because of the carboxyl moiety. We also excluded that **10** is simply toxic and thus does not support cell proliferation because the control cells that express ARTD10-G888W were unaffected by compound **10** (**Figure 2B**). This hypothesis was confirmed by a cellular thermal shift assays (CETSA), which showed that compound **10** did not support enhanced solubility of ARTD10 compared to the DMSO control, while **11** and **32** resulted in increased solubility of ARTD10 between 54°C and 56°C (**Fig. 2E**).

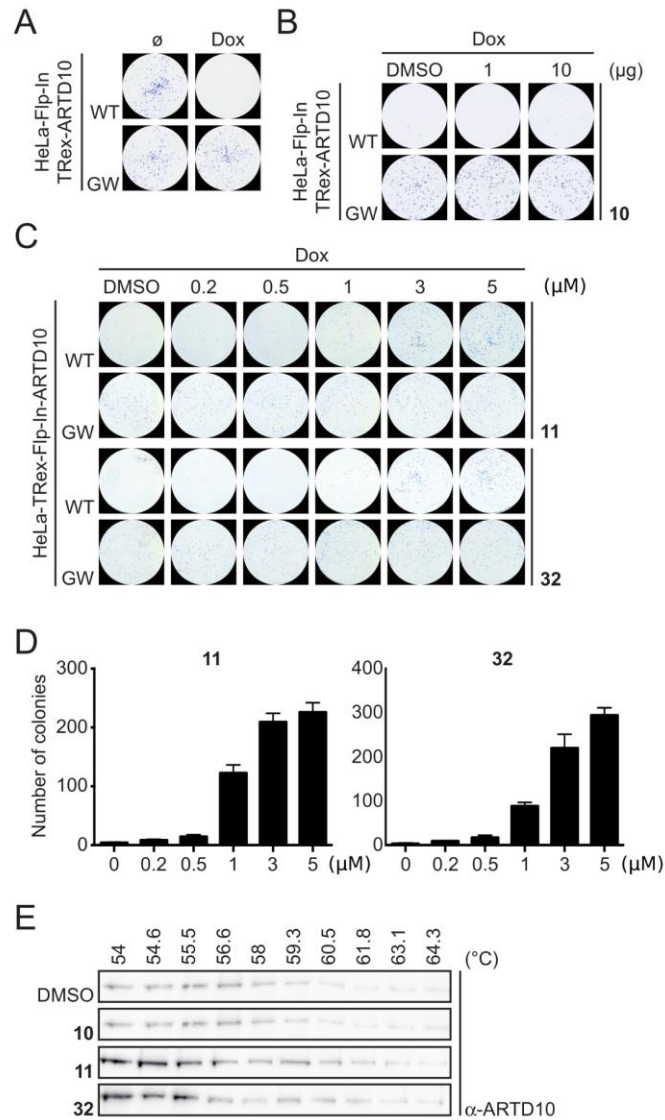


Figure 2. Rescue of ARTD10 overexpressing cells by compounds. **A-C)** HeLa cells (300/well) expressing doxycycline (Dox)-inducible constructs encoding ARTD10 (WT) or ARTD10-G888W (GW), which is catalytically inactive, were treated with 500 ng/ml Dox. After 10 days the cells were stained with methylene blue. Compounds **10**, **11** and **32** were added to the final concentrations indicated and replenished ever second day. Representative wells are shown. **D)** Colony formation experiments with compounds **11** and **32** were quantified. The data represent mean values of three experiments performed in duplicates with standard deviations. **E)** CETSA assays of U2OS cells incubated with the indicated compounds (10 µM) showing stabilization of ARTD10 by **11** and **32**, but not by **10**.

4. Discussion and Conclusions

In the current study we used the traditional approach of studying SAR by modifying an already reported potent ARTD10 inhibitor [17]. Based on the scaffold of compound **1**, we purchased, designed and synthesized new analogs. The strategy was to keep the nicotinamide mimicking benzamide constant for anchoring the compound to the binding site and to vary other parts of the molecule in order to better understand the interactions when the compound extends towards the new inhibitor binding site at the proximity of the so called acceptor site (**Figure 1**). The first modifications were to understand the minimum structural features needed for inhibition of ARTD10 and already with an *O*-linked small alkyl group we could measure micromolar IC₅₀ values. Together with the observed ARTD10 selectivity of the *O*-methyl derivative **3** (**Table 5**), this describes a key pharmacophore for an ARTD10 inhibitor. We then focused on modifying the linker region between the aromatic A- and B-rings. The analysis revealed that also an -OCH₂- linker in 4-(benzyloxy)benzamides could be useful for ARTD10 inhibition (**Table 3**). Potency of the 4-(benzyloxy)benzamides can be enhanced by the presence of a suitable substituent on the B-ring such as the *o*-fluorine that impart **32** an IC₅₀ of 230 nM for ARTD10 inhibition. All analyzed compounds showed selectivity towards ARTD10 over the other assayed enzymes of the human ARTD family suggesting that extending the compounds towards the acceptor site would be a way to create specific mARTD, at least ARTD10, inhibitors. The hydrophobic residue between the NAD⁺ binding site and the acceptor site is Ile987 in ARTD10 (**Figure 1C**) and the corresponding residue is hydrophobic in most mARTDs, in contrast to pARTDs, directly implying that it is possible to distinguish pARTD and mARTD inhibitors through the interactions at this location. Our study confirmed that not only **1**, but also a handful of analogs extending here are able to inhibit ARTD10 and not pARTDs. The compounds were directed towards ARTD10 and they indeed were selective towards ARTD10 over other mARTDs (**Table 5**). Therefore, further modification will be likely needed to develop specific inhibitors for other mARTDs from the 4-(phenoxy) and 4-(benzyloxy)benzamides.

The best compounds described here, **1**, **11** and **32**, are not only selective towards ARTD10, but are also nontoxic to cells. They enter cells and inhibit cellular ARTD10 rescuing the cells from ARTD10 induced cell death (**Figure 2**). They are therefore useful tools to study ARTD10 biology and the roles of ARTD10 in DNA repair, cellular signaling, and apoptosis.

5. Experimental Section

5.1. Chemistry

All starting materials were commercially available unless otherwise indicated. All commercially available starting materials, reagents, and solvents, including anhydrous solvents, were purchased from commercial sources and used as received. All reactions were routinely checked by thin-layer chromatography (TLC) using silica gel 60F₂₅₄ (Merck) and spots were visualized by exposure to ultraviolet light (UV) or iodine. After extraction, organic solutions were dried over anhydrous Na₂SO₄, filtered, and concentrated with a Büchi rotary evaporator at reduced pressure. Flash column chromatography was performed using Merck silica gel 60 (230-400 mesh). Yields are of purified product and were not optimized. ¹H NMR and ¹³C NMR spectra were acquired at 200 MHz (Bruker Avance DPX-200) or at 400 MHz (Bruker Avance DRX-400) using residual solvents signal such as chloroform ($\delta = 7.26$) or dimethylsulfoxide ($\delta = 2.48$) as an internal standard. Chemical shifts are reported in ppm (δ) and coupling constant are reported in hertz (Hz). The spectral data are consistent with the assigned structures. The spin multiplicities are indicated by the symbols s (singlet), d (doublet), dd (doublet of doublet), t (triplet), q (quartet), m (multiplet), and bs (broad singlet). Melting points were determined in capillary tubes (Büchi Electrothermal Mod. 9100) and are uncorrected. High-resolution mass spectra (HRMS) were recorded on Agilent Technologies 6540 UHD Accurate Mass Q-TOF LC/MS, HPLC 1290 Infinity using electrospray ionization (ESI) in the positive mode. Purity of the final compounds was determined by LC-MS on Agilent Technologies 6550 iFUNNEL Q-TOF equipped with HPLC 1290 Infinity with DAD detector and found to be $\geq 95\%$. HPLC

conditions to assess the purity of final compounds were as follows: column, Zorbax Eclipse Plus C12 Rapid Resolution HD 2.1x50mm (1.8 μ M); flow rate, 0.5 mL/min; acquisition time, 4 min, stop run at 6 min; DAD 190–650 nm; oven temperature, 50 °C; Eluent A: water +0.1% Formic Acid, Eluent B: Acetonitrile +0.1% Formic Acid, linear gradient B from (5%-95% in 4 min, stop run at 6 min). Compounds **2-6**, **8**, **10**, **20**, **23**, **24**, **25**, **27**, **28**, **32**, **34** were purchased from Enamine; **18**, **26**, **30**, **33** from Chembridge; **22** and **29** from Specs; **31** from Princeton and **4** from Combi-Blocks. Their purity was confirmed to be > 95% based on LC-MS. Compounds **7**, **9**, **11-17**, **19**, and **35** were instead synthesized as described below. Although the synthetic procedures used for the synthesis of compounds **7** [22] and **11** [23] were already reported, their characterization was reported here for the first time. For compounds **12** [24] and **41** [29] a different synthetic procedure was applied and herein described.

5.1.1. General procedure for nitriles hydration to amides

(Method A). To a solution of the appropriate nitrile (1.0 mmol) in DMSO (4 mL) cooled to 0 °C, K₂CO₃ (0.15 mmol) and aqueous 30% H₂O₂ solution (0.7 mL/mmol) were added. The reaction mixture was then stirred at room temperature until no starting material was detected by TLC. The mixture was diluted with water, yielding a precipitate that was filtered, washed with water, and purified as described below.

(Method B). A mixture of the appropriate nitrile (1.0 mmol) and H₂SO₄ conc (5 mL/mmol) was stirred at 60 °C until no starting material was detected by TLC. The reaction mixture was then poured into ice/water and added of saturated solution of NaHCO₃, yielding a precipitate that was filtered and purified as described below.

5.1.2. *4-(4-Methoxyphenoxy)benzamide (7)* [22]. The title compound was prepared through Method A (2.5 h). White crystals, mp 193-195 °C. ¹H NMR (400 MHz, DMSO-*d*₆): δ 3.65 (s, 3H, OCH₃), 6.85 (d, *J* = 7.9 Hz, 2H, aromatic CH), 6.95 and 7.05 (d, *J* = 8.1 Hz, each 2H, aromatic CH), 7.25 (bs,

1H, CONH₂), 7.75-7.85 (m, 3H, aromatic CH and CONH₂); ¹³C NMR (101 MHz, DMSO-*d*₆): δ 55.7, 115.5, 116.4, 121.7, 128.5, 129.9, 148.7, 156.4, 161.0, 167.5. HRMS (ESI) *m/z*: [M+H]⁺ calcd for C₁₄H₁₃NO₃, 244.0974; found 244.0963.

5.1.3. 4-(4-Hydroxyphenoxy)benzamide (9). To a solution of **7** (0.45 g, 1.85 mmol) in dry CH₂Cl₂ (4 mL), 1M solution of BBr₃ in CH₂Cl₂ (7.40 mL, 7.40 mmol) was added dropwise maintaining the temperature at 0 °C. The reaction mixture was stirred at room temperature for 4.5 h. Then, the mixture was quenched with MeOH and water and extracted with CH₂Cl₂. The organic layers were evaporated to dryness, yielding a residue that was purified by flash chromatography eluting with CHCl₃:MeOH (93:7), to give **9** (0.15 g, 36%) as white solid; mp 202-204 °C. ¹H NMR (400 MHz, DMSO-*d*₆): δ 6.75 (d, *J* = 8.7 Hz, 2H, aromatic CH), 7.85 (d, *J* = 8.5 Hz, 2H, aromatic CH), 7.90 (d, *J* = 8.7 Hz, 2H, aromatic CH), 7.20 (bs, 1H, CONH₂), 7.75-7.85 (m, 3H, aromatic CH and CONH₂), 9.50 (s, 1H, OH); ¹³C NMR (101 MHz, DMSO-*d*₆): δ 116.1, 116.7, 121.9, 128.3, 129.9, 147.2, 154.7, 161.3, 167.5. HRMS (ESI) *m/z*: [M+H]⁺ calcd for C₁₃H₁₁NO₃, 230.0818; found 230.0809.

5.1.4. 4-(4-Formylphenoxy)benzamide (11) [23]. The title compound was prepared through Method B. (1 h). White solid, mp 135-136 °C. ¹H NMR (400 MHz, DMSO-*d*₆): δ 7.10-7.20 (m, 4H, aromatic CH), 7.35 (bs, 1H, CONH₂), 7.80-7.90 (m, 4H, aromatic CH), 7.95 (bs, 1H, CONH₂), 9.95 (s, 1H, CHO); ¹³C NMR (101 MHz, DMSO-*d*₆): δ 118.8, 119.7, 130.3, 130.9, 132.2, 132.5, 157.8, 161.9, 167.4, 192.1. HRMS (ESI) *m/z*: [M+H]⁺ calcd for C₁₄H₁₁NO₃, 242.0818; found 242.0813.

5.1.5. 4-Phenoxybenzamide (12). The title compound was prepared starting from **38** through Method A (2 h) and purified by crystallization by EtOH/H₂O mixture, in 50% yield as white crystals; mp 177-178 °C. ¹H NMR (400 MHz, DMSO-*d*₆): δ 6.95 (d, *J* = 8.6 Hz, 2H, aromatic CH), 7.05 (d, *J* = 7.9 Hz, 2H, aromatic CH), 7.20 (t, *J* = 7.3 Hz, 1H, aromatic CH), 7.30 (bs, 1H, CONH₂), 7.40 (t, *J* = 7.8

Hz, 2H, aromatic CH), 7.80 (d, $J = 8.6$ Hz, 2H, aromatic CH), 7.90 (bs, 1H, CONH₂); ¹³C NMR (101 MHz, DMSO-*d*₆): δ 117.7, 119.9, 124.7, 129.4, 130.1, 130.6, 156.0, 159.9, 167.5. HRMS (ESI) m/z : [M+H]⁺ calcd for C₁₃H₁₁NO₂, 214.0869; found 214.0859.

5.1.6. 4-(Pyridin-2-yloxy)benzamide (13). The title compound was prepared starting from **40** [25] through Method B (1 h) and purified by crystallization by EtOH, in 37% yield as white crystals; mp 165-167 °C. ¹H NMR (400 MHz, DMSO-*d*₆): δ 7.05 (d, $J = 8.2$ Hz, 1H, aromatic CH), 7.15-7.20 (m, 3H, aromatic CH), 7.30 (bs, 1H, CONH₂), 7.80-7.90 (m, 3H, aromatic CH), 7.95 (bs, 1H, CONH₂), 8.10-8.20 (m, 1H, aromatic CH); ¹³C NMR (101 MHz, DMSO-*d*₆): δ 112.4, 119.9, 120.9, 129.6, 130.7, 140.8, 147.9, 156.8, 162.9, 167.7. HRMS (ESI) m/z : [M+H]⁺ calcd for C₁₂H₁₀N₂O₂, 215.0821; found 215.0829.

5.1.7. 4,4'-Iminodibenzoamide (14). The title compound was prepared starting from **41** [26] through Method A (5 min) and purified by crystallization by EtOH, in 40% yield as white crystals; mp 260-261 °C. ¹H NMR (200 MHz, DMSO-*d*₆): δ 7.05 and 7.70 (d, $J = 8.6$ Hz, each 6H, aromatic CH and CONH₂), 8.75 (s, 1H, NH); ¹³C NMR (101 MHz, DMSO-*d*₆) 116.3, 126.1, 129.5, 145.6, 167.8. HRMS (ESI) m/z : [M+H]⁺ calcd for C₁₄H₁₃N₃O₂, 256.1087; found 256.1082.

5.1.8. 4,4'-(Methylmino)dibenzamide (15). The title compound was prepared starting from **42** [27] through Method A (5 h) and purified by crystallization by EtOH/DMF mixture, in 55% yield as white crystals; mp 280-281 °C. ¹H NMR (200 MHz, DMSO-*d*₆): δ 3.25 (s, 3H, CH₃), 6.95 (d, $J = 8.7$ Hz, 4H, aromatic CH), 7.20 (bs, 2H, CONH₂), 7.70-7.80 (m, 6H, aromatic CH and CONH₂); ¹³C NMR (101 MHz, DMSO-*d*₆) 40.1, 119.7, 127.0, 129.3, 150.5, 168.1. HRMS (ESI) m/z : [M+H]⁺ calcd for C₁₅H₁₅N₃O₂, 270.1243; found 270.1234.

5.1.9. *4,4'-Thiodibenzamide (16)*. The title compound was prepared starting from **43** [28] through Method A (5 h) and purified by crystallization by EtOH/DMF mixture, in 17% yield as white crystals; mp 299 °C. ¹H NMR (400 MHz, DMSO-*d*₆): δ 7.30 (d, *J* = 8.2 Hz, 4H, aromatic CH), 7.40 (bs, 1H, CONH₂), 7.85 (d, *J* = 8.2 Hz, 4H, aromatic CH), 7.95 (bs, 2H, CONH₂); ¹³C NMR (101 MHz, DMSO-*d*₆) 129.1, 130.6, 133.7, 138.2, 167.5. HRMS (ESI) *m/z*: [M+H]⁺ calcd for C₁₄H₁₂N₂O₂S, 273.0698; found 273.0691.

5.1.10. *4-[(4-cyanophenyl)thio]benzamide (17)*. The title compound was prepared starting from **43** [28] through Method A (5 min) but using 0.1 mL/mmol of aqueous 30% H₂O₂ solution and purified by flash chromatography eluting with CHCl₃:MeOH (98:2), in 39% yield as white solid; mp 207 °C. ¹H-NMR (200 MHz, DMSO-*d*₆): δ 7.25 (d, *J* = 8.3, 2H, aromatic CH), 7.40 (bs, 1H, CONH₂), 7.50 (d, *J* = 8.2, 2H, aromatic CH), 7.70 (d, *J* = 8.3 Hz, 2H, aromatic CH), 7.85 (d, *J* = 8.2 Hz, 2H, aromatic CH), 8.00 (bs, 1H, CONH₂); ¹³C NMR (101 MHz, DMSO-*d*₆): 109.2, 119.0, 129.0, 129.4, 133.0, 133.5, 135.0, 135.1, 143.5, 167.4. HRMS: *m/z* calcd for C₁₄H₁₀N₂OS 255.0593 (M+H)⁺, found 255.0598.

5.1.11. *4-{[4-(Aminocarbonyl)benzyl]oxy}benzamide (19)*. The title compound was prepared starting from **44** through Method A (2.5 h) and purified by crystallization by DMF, in 36% yield as white crystals; mp 305-306 °C. ¹H NMR (400 MHz, DMSO-*d*₆): δ 5.20 (s, 2H, CH₂), 7.00 (d, *J* = 8.8 Hz, 2H, aromatic CH), 7.20 and 7.35 (bs, each 1H, CONH₂), 7.50 (d, *J* = 8.2 Hz, 2H, aromatic CH), 7.80 (d, *J* = 8.7 Hz, 3H, aromatic CH and CONH₂), 7.85 (d, *J* = 8.2 Hz, 2H, aromatic CH); ¹³C NMR (101 MHz, DMSO-*d*₆): δ 69.1, 114.6, 127.1, 127.6, 128.0, 129.7, 134.1, 140.3, 160.8, 167.7, 167.9. HRMS (ESI) *m/z*: [M+H]⁺ calcd for C₁₅H₁₄N₂O₃, 271.1083; found 271.1077.

5.1.12. *4-(2-Fluorophenoxy)benzamide (35)*. The title compound was prepared starting from **39**

through Method A (3 h) and purified by crystallization by cyclohexane/EtOAc mixture, in 68% yield as white crystals; mp 152-153 °C. ¹H NMR (400 MHz, DMSO-*d*₆): δ 6.90 (d, *J* = 8.7 Hz, 2H, aromatic CH), 7.20-7.30 (m, 4H, aromatic CH and CONH₂), 7.35-7.45 (m, 1H, aromatic CH), 7.85 (d, *J* = 8.8 Hz, 2H, aromatic CH), 7.90 (bs, 1H, CONH₂); ¹³C NMR (101 MHz, DMSO-*d*₆): δ 116.1, 117.8 (*J*_{H-F} = 17.9 Hz), 123.4, 126.1 (*J*_{H-F} = 3.7 Hz), 126.8 (*J*_{H-F} = 7.2 Hz), 129.4, 130.1, 142.2 (*J*_{H-F} = 11.6 Hz), 154.2 (*J*_{H-F} = 247.9 Hz), 159.8, 167.5. HRMS (ESI) *m/z*: [M+H]⁺ calcd for C₁₃H₁₀FNO₂, 232.0775; found 232.0764.

5.1.13. 4-[(Cyanobenzyl)oxy]benzotrile (**44**) [29]. To a solution of diisopropyl azodicarboxylate (DIAD) (0.35 mL, 1.76 mmol) in dry THF (10 mL), Ph₃P (1.3 g, 5.20 mmol) was added at 0 °C under N₂ atmosphere. The mixture was stirred until there was a white precipitate. Then, 4-hydroxybenzotrile (0.2 g, 1.67 mmol) and 4-(hydroxymethyl)benzotrile (0.23 g, 1.76 mmol) were added and the reaction mixture was maintained to room temperature overnight. The mixture was then poured into ice/water, yielding a precipitate that was filtered and treated with Et₂O, to give **44** (0.17 g, 44%) as white solid. ¹H NMR (400 MHz, DMSO-*d*₆): δ 5.25 (s, 2H, CH₂), 7.15 and 7.75 (d, *J* = 8.6 Hz, each 2H, aromatic CH), 7.65 and 7.85 (d, *J* = 8.0 Hz, each 2H, aromatic CH).

5.2. PAINS and aggregators filters.

The most active compounds (**1**, **10**, **11**, **20**, **32**,) were examined for known classes of pan-assay interference compounds (PAINS) [31] and aggregators by using the ZINC 15 remover filter at <http://zinc15.docking.org> [32]. None of the compounds were found as potential PAINS or aggregators.

5.3. Protein expression and purification

All proteins used in the current study were expressed in *E. coli*, and purified in using Ni-affinity and size exclusion chromatography according to our previously reported protocols [17]. The details of the constructs used for each ARTD enzyme are listed in **Table S1**.

5.4. Activity assay

Dose response experiments were carried out using our previously reported activity assay for mARTD enzymes [18]. Half log dilutions of inhibitors were used and reactions were performed in quadruplicates. IC₅₀ curves were fitted using sigmoidal dose response curve (four variables) in GraphPad Prism version 5.04 (GraphPad Software). Details of the assay conditions of different ARTD enzymes are available in **Table S1**.

5.5. Differential Scanning Fluorimetry

DSF experiments were carried out for ARTD9, ARTD10 and ARTD13. Protein used was diluted to 0.25 mg/ml in PBS. SyproOrange (Life Technologies) at a concentration of 5X was used as the reporter dye. The compound concentration used for the experiment was 100 μM. The experiments were repeated three times with appropriate control. It was performed on a real-time PCR machine (Applied Biosystems) with the temperature increasing from 21°C up to 90°C (70 cycles) with 1°C increment per minute.

5.6. Colony Formation and Cellular Thermal Stability Assay

The colony formation assays and the cellular thermal stability assays were performed precisely as described earlier [17]. The compounds were dissolved in DMSO and added to the final concentrations as indicated in the figure. New medium and compounds were added every other day.

5.7. Crystallization

ARTD7 (Y598L) was co-crystallized with **1** utilizing the existing crystallization conditions for ARTD7 [33]. Compound **1** (1.5 μ L of 10 mM in 100% DMSO) was mixed with 35 μ L of 11.7 mg/mL ARTD7 (Y598L) and incubated for 1 min at 20°C for crystallization. 150 nL of the protein-ligand solution was mixed with 75 nL of well solution consisting of 0.2 M NH₄Cl pH 7.5, 20% (w/v) PEG 3350. Crystals were grown in sitting drops using vapour-diffusion at 20°C and were obtained in 24 hours.

5.8. Data collection, processing and refinement

Prior to data collection, A crystal was cryoprotected with 0.7 μ L of 0.2 M NH₄Cl pH 7.5 in 30% (v/v) MPD (2-methyl-2,4-pentanediol), which was added to the drop containing a crystal. X-ray diffraction data were collected on beamline ID29 at ESRF (Grenoble, France). Data were processed and scaled with XDS program [34]. Phases for the structure of ARTD7 (Y598L) in complex with **1** were obtained by molecular replacement with Phaser [35] using the model of ARTD7 (PDB accession code 3BLJ) as a search model. The model was refined with REFMAC5 from CCP4 package. Model visualization and building was performed using Coot [36]. The residues in the model were numbered according to the canonical sequence of UniProt entry Q460N3-1. Data collection and refinement statistics are shown in the **Table S2**.

5.9. Docking

Docking was performed using the GOLD program [37] with the Chemscore scoring function. The crystal structure of ARTD10 (PDB accession code 3HKV) was used as a template. The binding pocket was defined with a 6 Å radius based on 3-aminobenzamide ligand present in the crystal structure.

Acknowledgements

This work was funded by Sigrid Jusélius foundation, Biocenter Oulu, Jane and Aatos Erkkö

Foundation, Academy of Finland (grant no. 287063 and 294085 for LL), German Research Foundation DFG (LU466/16-1 to BL), start-up program of the Excellence Initiative of the RWTH Aachen University (StUpPD_119_13 to PV), and the START program of the Faculty of Medicine, RWTH Aachen University (117/15 to PV). The use of the facilities and expertise of the Biocenter Oulu X-ray crystallography and proteomics core facilities are gratefully acknowledged. We acknowledge the technical support by Barbara Lippok. We also thank SGC, Stockholm for some of the ARTD expression constructs and the COST action CA15135 (Multi-Target Paradigm for Innovative Ligand Identification in the Drug Discovery Process, MuTaLig) for support.

Appendix A. Supplementary data

Supplementary material contains details of the protein constructs, activity assay conditions, data collection and refinement statistics. The material also contains figures showing structural comparisons, docking of the compounds, differential scanning fluorimetry data, and the ¹H NMR and ¹³C NMR spectra of the synthesized target compounds.

PDB Deposition

Coordinates and structure factors are deposited to the protein data bank with the accession code 6EK3.

Author Information

Corresponding author

*Phone: +358 2 9448 1169; E-mail: lari.lehtio@oulu.fi

Conflict of Interest

Y.N. and L.L. declare that they are partners and own shares of the company Fangorn Biopharma Oy and its subsidiary ARTD Therapeutics Oy focusing on the development of mARTD inhibitors.

References

- [1] M. Bütepage, L. Eckeï, P. Verheugd, B. Lüscher, Intracellular mono-ADP-ribosylation in signaling and disease, *Cells* 4 (2015) 569–595.
- [2] S. Till, K. Diamantara, A.G. Ladurner, PARP: A transferase by any other name, *Nat. Struct. Mol. Biol.* 15 (2008) 1243–1244.
- [3] M.O. Hottiger, P.O. Hassa, B. Lüscher, H. Schüler, F. Koch-Nolte, Toward a unified nomenclature for mammalian ADP-ribosyltransferases, *Trends Biochem. Sci.* 35 (2010) 208–219.
- [4] H. Otto, P.A. Reche, F. Bazan, K. Dittmar, F. Haag, F. Koch-Nolte, In silico characterization of the family of PARP-like poly(ADP-ribosyl)transferases (PARTs), *BMC Genomics* 6 (2005) 139.
- [5] H. Kleine, E. Poreba, K. Lesniewicz, P.O. Hassa, M.O. Hottiger, D.W. Litchfield, B.H. Shilton, B. Lüscher, Substrate-assisted catalysis by PARP10 limits its activity to mono-ADP-ribosylation, *Mol. Cell* 32 (2008) 57–69.
- [6] R. Gupte, Z. Liu, W.L. Kraus, PARPs and ADP-ribosylation: recent advances linking molecular functions to biological outcomes, *Genes Dev.* 31 (2017) 101–126.
- [7] E.S. Scarpa, G. Fabrizio, M.A. Di Girolamo, A role of intracellular mono-ADP-ribosylation in cancer biology, *FEBS J.* 280 (2013) 3551–3562.
- [8] B. Lüscher, M. Bütepage, L. Eckeï, S. Krieg, P. Verheugd, B.H. Shilton, ADP-ribosylation, a multifaceted posttranslational modification involved in the control of cell physiology in health and disease, *Chem. Rev.* 118 (2017) 1092–1136.
- [9] M. Yu, S. Schreek, C. Cerni, C. Schamberger, K. Lesniewicz, E. Poreba, J. Vervoorts, G. Walsemann, J. Grötzinger, E. Kremmer, Y. Mehraein, J. Mertsching, R. Kraft, M. Austen, J. Lüscher-Firzlaff, B. Lüscher, PARP-10, a novel Myc-interacting protein with poly(ADP-

- ribose) polymerase activity, inhibits transformation, *Oncogene* 24 (2005) 1982–1993.
- [10] G.T. Marsischky, B.A. Wilson, R.J. Collier, Role of glutamic acid 988 of human poly-ADP-ribose polymerase in polymer formation. evidence for active site similarities to the ADP-ribosylating toxins, *J. Biol. Chem.* 270 (1995) 3247–3254.
- [11] C.M. Nicolae, E.R. Aho, A.H.S. Vlahos, K.N. Choe, S. De, G.I. Karras, G.-L. Moldovan, The ADP-ribosyltransferase PARP10/ARTD10 interacts with proliferating cell nuclear antigen (PCNA) and is required for DNA damage tolerance, *J. Biol. Chem.* 289 (2014) 13627–13637.
- [12] N. Herzog, J.D.H. Hartkamp, P. Verheugd, F. Treude, A.H. Forst, K.L.H. Feijs, B.E. Lippok, E. Kremmer, H. Kleine, B. Lüscher. Caspase-dependent cleavage of the mono-ADP-ribosyltransferase ARTD10 interferes with its pro-apoptotic function, *FEBS J.* 280 (2013) 1330–1343.
- [13] H. Kleine, A. Herrmann, T. Lamark, A.H. Forst, P. Verheugd, J. Lüscher-Firzlauff, B. Lippok, K.L. Feijs, N. Herzog, E. Kremmer, T. Johansen, G. Müller-Newen, B. Lüscher, Dynamic subcellular localization of the mono-ADP-ribosyltransferase ARTD10 and interaction with the ubiquitin receptor P62, *Cell Commun. Signal.* 10 (2012) 28.
- [14] K.L. Feijs, H. Kleine, A. Braczynski, A.H. Forst, N. Herzog, P. Verheugd, U. Linzen, E. Kremmer, B. Lüscher, ARTD10 substrate identification on protein microarrays: regulation of GSK3 β by mono-ADP-ribosylation, *Cell Commun. Signal.* 11 (2013) 5.
- [15] P. Verheugd, A.H. Forst, L. Milke, N. Herzog, K.L.H. Feijs, E. Kremmer, H. Kleine, B. Lüscher, Regulation of NF- κ B signalling by the mono-ADP-ribosyltransferase ARTD10, *Nat. Commun.* 4 (2013) 1683.
- [16] M.A. Shahrour, C.M. Nicolae, S. Edvardson, M. Ashhab, A.M. Galvan, D. Constantin, B. Abu-Libdeh, G.-L. Moldovan, O. Elpeleg, PARP10 deficiency manifests by severe developmental delay and DNA repair defect, *Neurogenetics* 17 (2016) 227–232.
- [17] H. Venkannagari, P. Verheugd, J. Koivunen, T. Haikarainen, E. Obaji, Y. Ashok, M. Narwal,

- T. Pihlajaniemi, B. Lüscher, B.; L. Lehtiö, Small-molecule chemical probe rescues cells from mono-ADP-ribosyltransferase ARTD10/PARP10-induced apoptosis and sensitizes cancer cells to DNA damage, *Cell Chem. Biol.* 23 (2016) 1251–1260.
- [18] H. Venkannagari, A. Fallarero, K.L.H. Feijs, B. Lüscher, L. Lehtiö, Activity-based assay for human mono-ADP-ribosyltransferases ARTD7/PARP15 and ARTD10/PARP10 aimed at screening and profiling inhibitors, *Eur. J. Pharm. Sci.* 49 (2013) 148–156.
- [19] A. Ruf, G. de Murcia, G.E. Schulz, Inhibitor and NAD⁺ binding to poly(ADP-ribose) polymerase as derived from crystal structures and homology modeling, *Biochemistry* 37 (1998) 3893–3900.
- [20] S. Yang, C. Wu, M. Ruan, Y. Yang, Y. Zhao, J. Niu, W. Yang, J. Xu, Metal- and ligand-free Ullmann-type C–O and C–N coupling reactions promoted by potassium *tert*-butoxide, *Tetrahedron Lett.* 53 (2012) 4288–4292.
- [21] B. Li, R. Pai, S.C. Cardinale, M.M. Butler, N.P. Peet, D.T. Moir, S. Bavari, T.L. Bowlin, Synthesis and biological evaluation of botulinum neurotoxin a protease inhibitors, *J. Med. Chem.* 53 (2010) 2264–2276.
- [22] J. Clayton, F. Ma, B. Van Wagenen, R. Ukkiramapandian, I. Egle, J. Empfield, M. Isaac, A. Slassi, G. Steelman, R. Urbanek, S. Walsh, Preparation of isoindolones as metabotropic glutamate receptor potentiators, (2006) WO2006020879.
- [23] B.B. Chen, H. Chen, M.A. Russell, J.M. Miyashiro, J.W. Malecha, T.D. Penning, Preparation of LTA4 hydrolase inhibitors, (1998) WO9840364.
- [24] M.J. Blanco-Pillado, M.D. Chappell, M. Garcia De la Torre, N. Diaz Buezo, J.E. Fritz, W.G. Holloway, J.E.Jr. Matt, C.H. Mitch, C. Pedregal-Tercero, S.J. Quimby, M.G. Siegel, D.R. Smith, R.D. Stucky, K. Takeuchi, E.M. Thomas, C.N. Wolfe, Preparation of [(aminoalkyl)aryl]oxy]nicotinamides and analogs as opioid receptor antagonist for treatment of obesity and related conditions, (2004) WO2004026305.

- [25] I. Güell, X. Ribas, Ligand-free Ullmann-type C–heteroatom couplings under practical conditions, *Eur. J. Org. Chem.* 2014 (2014) 3188–3195.
- [26] S. Mobashery, P.I. O'Daniel, M. Chang, Preparation of oxadiazole derivatives as antibacterial agents, (2009) WO2009041972.
- [27] J.H. Gorvin, The synthesis of di- and tri-arylamines through halogen displacement by base-activated arylamines: comparison with the Ullmann condensation, *J. Chem. Soc. [Perkin 1]* 0 (1988) 1331–1335.
- [28] T. Murase, M. Fujita, Highly blue luminescent triazine–amine conjugated oligomers, *J. Org. Chem.* 70 (2005) 9269–9278.
- [29] Chen, H.-Y.; Peng, W.-T.; Lee, Y.-H.; Chang, Y.-L.; Chen, Y.-J.; Lai, Y.-C.; Jheng, N.-Y.; Chen, H.-Y, Use of Base Control To Provide High Selectivity between Diaryl Thioether and Diaryl Disulfide for C–S Coupling Reactions of Aryl Halides and Sulfur and a Mechanistic Study, *Organometallics* **2013**, 32, 5514–5522.
- [30] D.A. Patrick, S.A. Bakunov, S.M. Bakunova, S.K. Jones, T. Wenzler, T. Barszcz, A. Kumar, D.W. Boykin, K.A. Werbovetz, R. Brun, Synthesis and antiprotozoal activities of benzyl phenyl ether diamidine derivatives, *Eur. J. Med. Chem.* 67 (2013) 310–324.
- [31] J.B. Baell, G.A. Holloway, New substructure filters for removal of pan assay interference compounds (PAINS) from screening libraries and for their exclusion in bioassays, *J. Med. Chem.* 53 (2010) 2719–2740.
- [32] T. Sterling, J.J. Irwin, ZINC 15 – Ligand discovery for everyone, *J. Chem. Inf. Model.* 55 (2015) 2324–2337.
- [33] T. Karlberg, M. Klepsch, A.-G. Thorsell, C.D. Andersson, A. Linusson, H. Schüler, Structural basis for Lack of ADP-ribosyltransferase activity in poly(ADP-ribose) polymerase-13/Zinc finger antiviral protein, *J. Biol. Chem.* 290 (2015) 7336–7344.
- [34] W. Kabsch, Integration, scaling, space-group assignment and post-refinement. *Acta*

Crystallogr. D Biol. Crystallogr. 66 (2010) 133–144.

- [35] A.J. McCoy, R.W. Grosse-Kunstleve, P.D. Adams, M.D. Winn, L.C. Storoni, R.J. Read, Phaser crystallographic software, *J. Appl. Crystallogr.* 40 (2007) 658–674.
- [36] P. Emsley, K. Cowtan, Coot: model-building tools for molecular graphics, *Acta Crystallogr. D Biol. Crystallogr.* 60 (2004) 2126–2132.
- [37] G. Jones, P. Willett, R.C. Glen, A.R. Leach, R. Taylor, Development and validation of a genetic algorithm for flexible docking, *J. Mol. Biol.* 267 (1997) 727–748.